THE JOURNAL OF PHYSICAL CHEMISTRY C

Article

Cite This: J. Phys. Chem. C 2019, 123, 27690−27696

pubs.acs.org/JPCC

Water Transport through Ultrathin Nanopores with Highly Polar Rims

Haiqi Gao,[†,‡] Qi Shi,[†] Petr Král,[*,‡] and Ruifeng Lu[*,†]

[†]Department of Applied Physics, Nanjing University of Science and Technology, Nanjing 210094, People's Republic of China

[‡]Department of Chemistry, University of Illinois at Chicago, Chicago, Illinois 60607, United States

Supporting Information

ABSTRACT: Molecular dynamics simulations are used to study water transport through nanopores with highly polar rims formed in atomically thin membranes, where the partial charges are determined by the types of atoms and chemical groups attached at the nanopore rims. Our simulations reveal that the dynamics of water passing through nanopores can be dramatically affected by its Coulomb coupling with the nanopore rims. Highly polar rims, especially with negatively charged edge atoms, can transiently bind neighboring waters by hydrogen bonds and help them pass through the nanopores, which can increase the effective cross-sections of nanopores for passing water. On the other hand, strong binding of water to the rims can block its transport through the nanopores. These observations can be implemented in designs of synthetic nanopores with a controllable molecular transport.

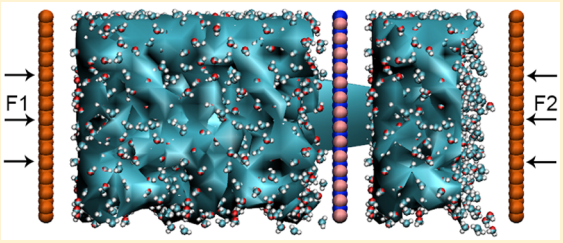

I. INTRODUCTION

In a modern society, population growth, pollution of the environment, and industrialization cause water shortage.[1] The fast and efficient gain of fresh water becomes crucial in addressing the developing water crisis.[2] Atomically thin membranes, possessing remarkable mechanical properties, energy efficiency, and environmentally friendly merit, have a huge application prospect in desalination.[3] In recent years, atomically thin membranes based on nanoporous graphene and related two-dimensional (2D) materials were thoroughly investigated.[4−7] Such ultrathin membranes can be designed to be used in water desalination,[6−14] water cleaning,[15] and ion separation.[4,16−20] The passage rates of molecular species through synthetic nanopores are affected by many parameters, such as the size, shape, polarity, and overall topology of nanopores. For example, charged and polar chemical groups attached to nanopores can affect the passage rates of ions[4] and polar molecules.[21−25] In particular, charged residues attached to carbon nanotubes (CNTs) can suppress water flow, since polar water molecules can be subjected to larger frictions with functionalized CNT walls.[21,23] Partial atomic charges present in boron-nitride nanotubes can also block water slippage,[24] which can result in about a 3-fold larger friction coefficient on boron-nitride sheet compared to graphene.[26]

In contrast to nanotubes, atomically thin nanoporous membranes interact with water molecules only over short passage distances. Moreover, water molecules passing ultrathin nanoporous membranes do not form relatively stable chains as in carbon nanotubes.[5] Partial atomic charges potentially present at membrane rims can change water passage through the membranes,[22,27] but no studies have systematically explored the roles played by large rim charges in water transport across the membrane,[28] so the underlying mechanisms are not very clear. However, this knowledge is necessary for guiding industrial desalination and water cleaning. To systematically investigate such phenomena, we use molecular dynamics (MD) simulations to study water transport through atomically thin nanopores with highly polar rims.

II. MODEL AND METHOD

The simulated system formed by a nanoporous membrane and two separated water reservoirs[28] is shown in Figure S1e in the Supporting Information. During the simulations, two sliding but otherwise rigid graphene pistons maintain constant pressures of 100 and 0.1 MPa in the left (feed) and right (permeate) reservoirs, respectively,[6,8,28] which induces a water flow from the left to the right reservoirs. A constant pressure difference between the two sides of the membrane is generated by applying a constant external force (f oriented in the z-direction) on each atom of the graphene pistons.[29] This generates on each side of the membrane a pressure of $\Delta P = nf/A$ (feed: 100 Mpa, permeate: 0.1 Mpa), where n is the number of C atoms in each piston (448 C) and A is the piston area (3.47×3.51 nm^2). The exerted constant external forces on each atom of the left and right side pistons are $f = 2.147 \times 10^{-12}$ and 2.147×10^{-15} N, respectively. Such a hydrostatic pressure algorithm can achieve constant pressure and induce steady-state flow in low-temperature argon liquid[30,31] and near room-temperature water liquid.[32] This and other methods have

Received: September 30, 2019
Published: October 7, 2019

DOI: 10.1021/acs.jpcc.9b09238
J. Phys. Chem. C 2019, 123, 27690−27696

been widely used in nonequilibrium molecular dynamics simulations.[6,8,33−35]

The MD simulations are carried out with Gromacs2016.3,[36] where water is modeled using the TIP4P potential[37] (see Table S1). The van der Waals (vdW) interactions and short-range repulsions between i and j atoms are modeled by Lennard-Jones (LJ) interactions with a cutoff of 1.4 nm and evaluated by the Lorentz−Berthelot rules, $\varepsilon_{ij} = (\varepsilon_i\varepsilon_j)^{1/2}$ and $\sigma_{ij} = (\sigma_i + \sigma_j)/2$, where ε_{ij} is the effective well depths and σ_{ij} is the minima positions. The electrostatic interactions are evaluated by the particle-mesh Ewald method[38] with a grid spacing of 0.12 nm. The simulations are carried in an NVT ensemble with periodic boundary conditions imposed. Initially, the systems are energy minimized, using the steepest descent method, and thermalized at T = 298 K. A velocity-rescale[39] thermostat was used to remove the excess heat to keep a kinetic constant temperature. Although this thermostat is not Galilean-invariant, it can be used in nonequilibrium water transport (see the Supporting Information).[40] Each system is independently simulated three times for 20 ns with a time step of 1 fs. The results are visualized using Visual Molecular Dynamics.[41] The average velocity of water and the number of hydrogen bonds among water molecules along the z-direction are calculated by an in-house code (see the Supporting Information for details).

III. RESULTS AND DISCUSSION

First, we simulate the water flow through fluoride- and hydrogen-passivated nanopores formed in graphene, called F-pore and H-pore, respectively, shown in Figure 1a,b. The

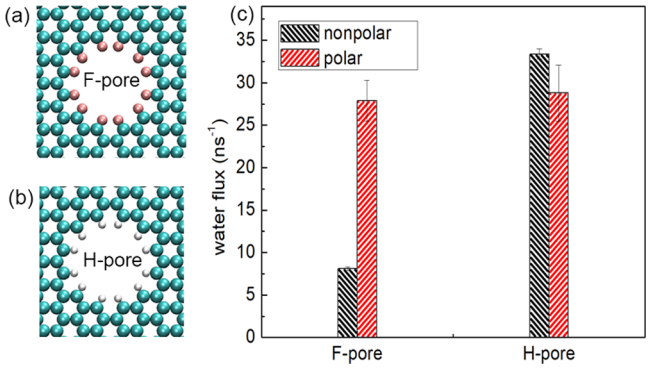

Figure 1. (a) F-pore. (b) H-pore. (c) The water flux through F- and H-pores with and without charge.

(positive) hydrogen, (negative) fluoride and carbon atomic charges (only first neighbors of H and F are polarized) are used as in previous studies[6,7,16] (shown in Table S1), giving overall neutral nanopores. To understand the effect of nanopore polarity on water transport, we also simulate the water flow through a nonpolar version of F- and H-pores, where all of the partial atomic charges are set to zero.

Figure 1c shows the water flux through all these nanopores with spatially fixed atoms. When the partial charges of the rim atoms were removed (nonpolar pores), the water flux through the H-pore is much larger than through the F-pore. The small flux in this F-pore is caused by steric effects due to bulkier F atoms (LJ parameters) and longer C−F bond lengths, as compared to the H-pore[42] (shown in Table S1). The geometric diameters of the F-pore and H-pore are 0.757 and 0.804 nm, respectively. The larger vdW radius of the F atom leads to a smaller effective cross-section for water passage than in the H-pore (Figure S2b,c). More water molecules can enter into the unpolarized H-pore than the F-pore under the same pressure (Figure S2a) and pass the membrane. In the polar pores the situation is very different. In the polar F-pore, the water flux dramatically increases. However, in the polar H-pore, the water flux is slightly decreased. Therefore, the polar F- and H-pores of different sizes provide a similar water flux, which indicates that the partial atomic charges at their rims have a great influence on this water transport. Our results are consistent with previous works for the weakly charged graphene pores.[34,35]Better understanding of these charge effects on water passage can promote applications in desalination[8,10,28,33] and water purification,[43,44] using molybdenum disulfide[33] and boron-nitride[28] membranes.

To understand how the water flux can be affected by large charges present at nanopores rims, we simulate next a water flow through triangular nanopores formed in hexagonal boron-nitride-type membranes with model atomic charges. The model charges of B-type and N-type atoms are varied in a range of $|q|$ = 0−1 e/atom (Table S1), but their LJ parameters are used as in boron and nitrogen atoms, respectively.[28,45] The triangular nanopores[46] are terminated by negatively or positively (Figure 2b inset) charged atoms and classified

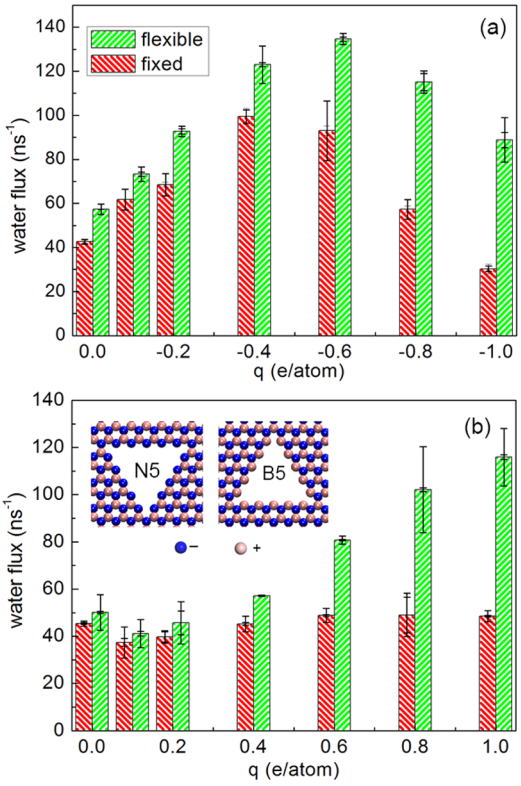

Figure 2. Water fluxes passing through fixed and flexible nanopores in (a) N5 and (b) B5 nanopores with a different polarity.

according to the number of terminal atoms on each of their sides (N4, N5, B4, B5, ...). Since these pores are charged (uneven removal of equally charged atoms, shown in the Supporting Information), the membranes are neutralized by discharging some atoms at the membrane periphery.

Figure 2 shows the water fluxes through fixed and flexible N5 (top) and B5 (bottom) nanopores with different partial atom charges; the results for B4 and N4 nanopores are shown in Figure S4. The water flux is expressed as the net number of

DOI: 10.1021/acs.jpcc.9b09238
J. Phys. Chem. C 2019, 123, 27690−27696

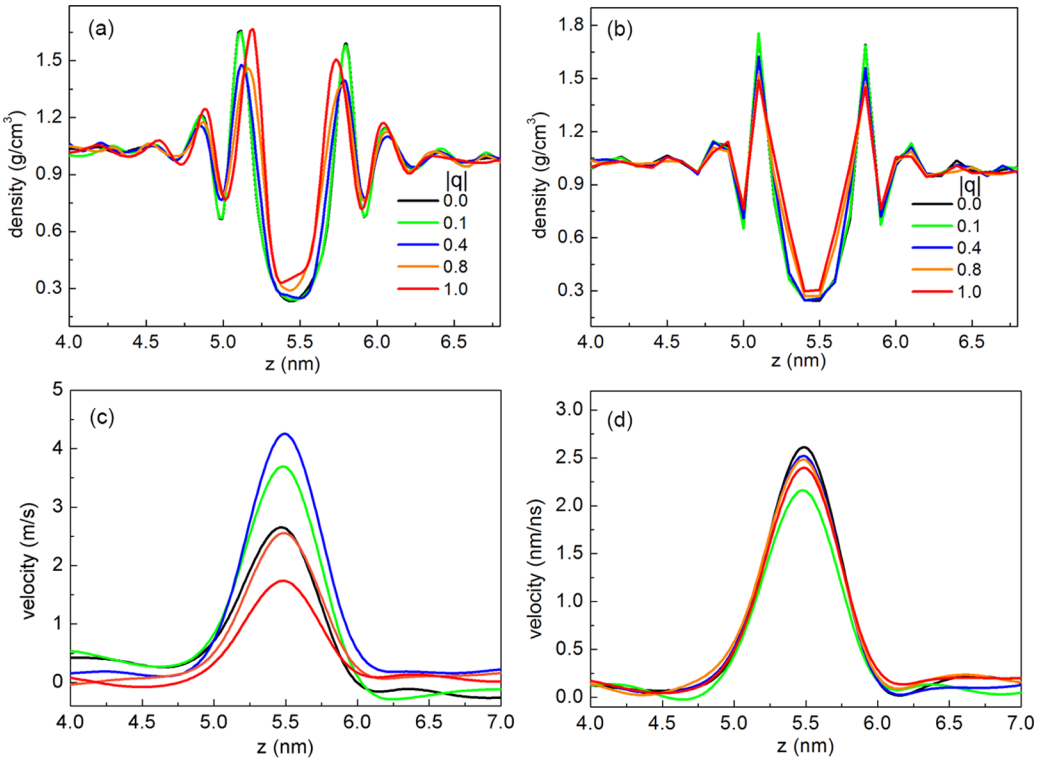

Figure 3. Water density along the *z*-direction for (a) N5, (b) B5 fixed membranes (only water molecules in the volume within the pore area along the *z*-direction are considered). The average velocities of water molecules diffusing through (c) N5, (d) B5 fixed membranes.

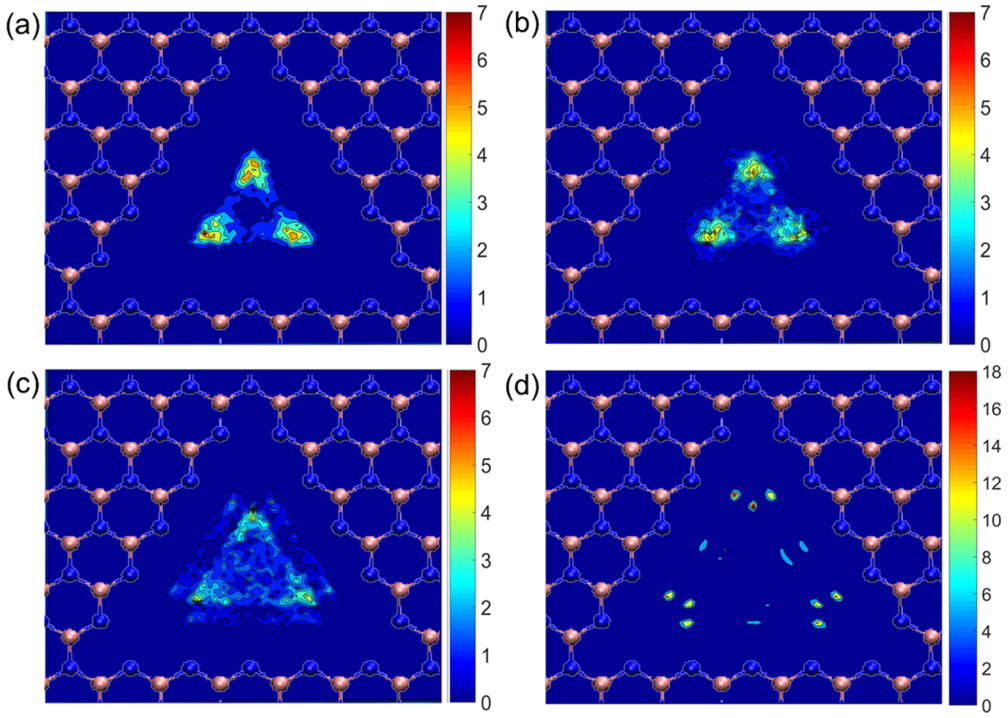

Figure 4. Water density distribution in the radial direction in the fixed N5 pore at (a) $|q|$ = 0 e/atom; (b) $|q|$ = 0.2 e/atom; (c) $|q|$ = 0.4 e/atom; (d) $|q|$ = 1.0 e/atom.

water molecules across the pore per unit time. In general, fluxes across the flexible nanoporous membranes are larger than those across the corresponding fixed membranes, especially for smaller nanopores and larger atomic charges. Figure 2a shows that the water flux through the negatively charged N5 pores first grows with the increasing atomic charges, reaches a maximum at charges of the nitrogen atoms q = −0.4 and −0.6 e/atom for the fixed and flexible membranes, respectively, and then drops again. A similar trend can be observed in the N4 pores (Figure S4a). The maximum flux in the negatively charged N5 pores is about twice larger than in the neutral pores. In contrast, in positively charged B5 pores,

DOI: 10.1021/acs.jpcc.9b09238
J. Phys. Chem. C 2019, 123, 27690−27696

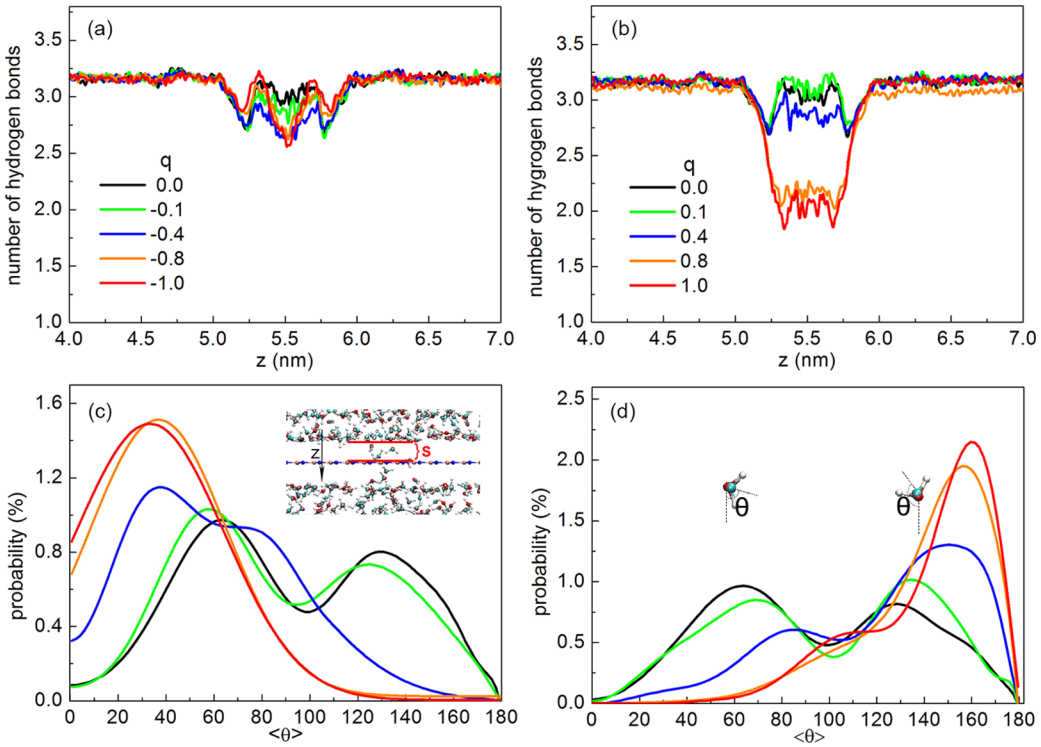

Figure 5. Average number of hydrogen bonds per water along the z-direction for (a) fixed N5 and (b) B5 pores. The dipole orientation probability of water molecules inside the short channel, which is between the membrane and the feed bulk (the region S of the inset c) for (c) fixed N5 pore and (d) B5 pore.

the flux increases only at high charging in flexible pores, as shown in Figure 2b. These results match similar trends observed in the F- and H-pores, where only the negative charging increases the water flux (see Figure 1c).

More simulations have been done with different pressure differences (Figure S5), but the charge has a asimilar effect on water transport at high pressures. One important metric for the performance of a membrane is a permeability, $P_w = \frac{F_w \cdot M_w}{A \cdot \Delta p \cdot N_0}$, where N_0 is the Avogadro constant, F_w is the water flux, M_w is the molecular weight of water, A is the effective area of the membrane estimated by assuming that the porosity of the membrane is 10%,[6] and Δp is the pressure difference. Based on the steady-state flow obtained in different pores at the standard pressure difference (Figure S3) at simulation times from 2 to 12 ns, P_w is calculated and shown in Figure S6. There is a local maximum seen in P_w at large negative charges, while P_w keeps slowly growing at large positive charges, in contrast to earlier studies.[34,35] These results sumarize the data obtained in Figure 2, revealing that larger crossections for passing waters could be seen in pores with negatively medium-charged rims.

To clarify more these observations, we need to perform further analysis of the conditions present within the nanopores. In general, a molecular flux through a pore is determined by a product of a fluid average density (ρ), average velocity (v) in the pore, and the pore effective cross-section (σ). When the passing molecules are polar, all of these properties can be controlled to some extent by the charge at the pore rim. Figure 3a displays the average ρ for water along the z-axis going through a fixed N5 pore. When the partial charges grow, the pores become more hydrophilic and ρ within the pores slightly increases.[47−49] Figure 3c shows that v averaged over these pores grows until $|q| \approx 0.4$ e/atom and then it sharply decreases. A similar situation is present in the fixed B5 pore, as shown in Figure 3b,d. However, here, the average v does not have a maximum at medium pore charges, like in the fixed N5 pore.

Our simulations reveal that the coupling of water to the rim can change the effective cross-section σ of the nanopore (Figure 4). To quantify this coupling, we calculate the Coulomb interaction energy ($E_{w\text{-}m}$) between water molecules and fixed membrane atoms near the pore (Figure S8). In Figure 5a,b, the calculated average number of hydrogen bonds between waters (per water molecule) is provided as a function of z coordinate passing through the pore. Note that during the pore passage, water molecules first need to break their hydrogen bonds with bulk water, before being able to pass.[35,50] For the N5 pore with a low negative charging, $E_{w\text{-}m}$ (Figure S8) is too small to cause many water molecules to be simultaneously caught by the nanopore (Figure 3a). However, the affinity between hydrogen atoms of water molecules and negative charges of the pore rim suppresses the number of hydrogen bonds present in water around the pore (Figure 5a). For N5 pores with a large enough negative charging, more fluctuating hydrogen atoms of water molecules can be caught by the rim (Figure S8). Therefore, σ also increases (Figure 4a−c). These partly trapped waters tend to pass through the pore with a larger effective cross-section by a rotation dynamics. When the rim atoms are more polar ($q > -0.6$), stronger Coulomb forces (Figure S8) draw water close to the pore edge, resulting in smaller σ (Figure 4d).

In contrast, the positive charges on the rim atoms impede the hydrogens of water molecules from entering into the pore and slightly increase the number of hydrogen bonds after water molecules flip into the pore region (Figure 5b). At the same time, the oxygen atoms of water can be caught only at a smaller

DOI: 10.1021/acs.jpcc.9b09238
J. Phys. Chem. C 2019, 123, 27690−27696

distance (middle water atom), which is not associated with a significant increase of the pore cross-section (Figure S7). When the rim atoms are more positively charged, stronger Coulomb attraction (Figure S8) takes water molecules from bulk into the pore region while breaking many hydrogen bonds (Figure 5b). This, in principle, can block the pore, so the flux should decrease. However, due to the presence of negatively charged neighboring atoms, the blocking is not so obvious (Figure 2b) like in the case of opposite charging. However, this water catching can be increased in flexible pores.

The transmembrane water passage can be nicely illustrated on trajectories of a few randomly selected oxygen atoms of water molecules that flip into the pore center. Figure 6 shows

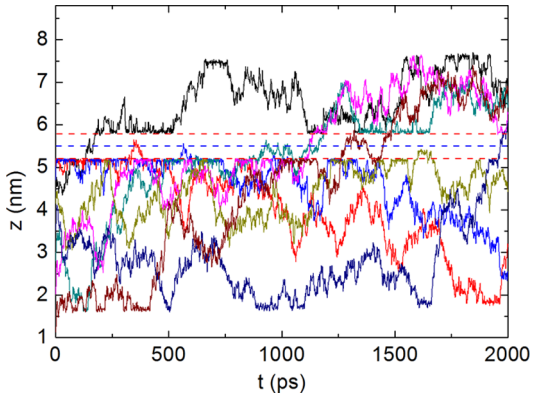

Figure 6. Trajectories of a few randomly selected oxygen atom in water molecules entering into the nonpolar fixed N5 pore. The fixed N5 membrane located in the blue line and between the red line is a volume layer.

randomly selected oxygen atom trajectories for the fixed N5 pore. Note that the region between the red lines is the volume excluded by the ultrathin membrane to form a short transport channel. The water molecule first flips into the channel and then completes its passage. Some water molecules will come back to the feed side and do not complete their passage. Figure 7 shows the total number of water molecules flipping into the channel (N_{wt}), the number of water molecules passing through the nanopore to the permeate side (N_{wp}), the number of water molecules that come back to the feed side (N_{wr}), and the transmembrane probability (P_T) defined as $P_T = \frac{N_{wp}}{N_{wt}}$ at the first 10 ns (steady-state flow). Interestingly, in N5 about half of the water molecules entereing into the channel return to the feed side. Over there, the N_{wt}, N_{wp}, N_{wr}, and P_T values are all initially proportional to the charge and begin to decrease at |q| = 0.5 e/atom (Figure 7a). In B5 the N_{wt}, N_{wp}, and N_{wr} values slightly decrease as the rim positive charge increases ($q \leq 0.5$ e/atom), but at larger charges N_{wt} and N_{wr} quickly increase. However, N_{wf} keeps constant at large charges, while P_T always drops at large charges.

To better understand the water passage dynamics, the dipole orientations of water molecules inside the channel between the feed bulk and membrane (the inset in Figure 5c) are studied at different rim polarities. Here, $\langle\theta\rangle$ is defined as the angle between a water dipole (oxygen atom to the center of two hydrogen atoms) and the z-direction. Unlike carbon nanotubes, where water dipole orientations have special values,[51] $\langle\theta\rangle$ in our simulations mostly ranges from 0 to 180°, with two peaks around 60 and 130° for the unpolarized fixed N5 and B5

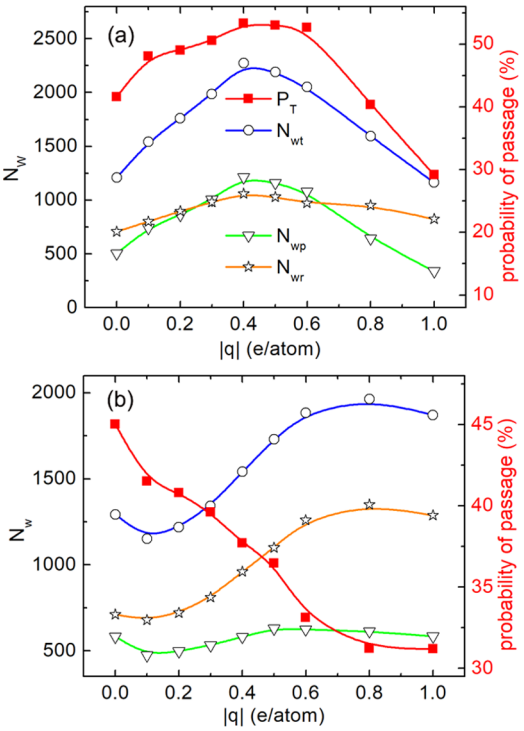

Figure 7. Total number of water molecules flipping into the channel (N_{wt}), the number of water molecules passingthrough the nanopore to the permeate side (N_{wp}), the number of water molecules coming back to the feed side (N_{wr}), and the transmembrane probability (P_T) during the initial 10 ns (steady-state flow) for the (a) fixed N5 and (b) fixed B5 membrane.

pores (Figure 5c,d). This means that water molecules frequently flip in the nanopores.[5,35] Since the center of mass of a water molecule is mostly localized on its oxygen atom, the hydrogen atoms in water molecules tend to rotate fast around it and they are more likely to enter nanopores.[35] The behavior of water molecules is very sensitive to the presence of Coulomb forces in such a short channel. For convenience, we define $0 < \langle\theta\rangle < 90°$ as +dipole states and the angles larger than that but smaller than 180° are set as −dipole states.[51] Figure 5c shows that water molecules prefer +dipole states with the increasing negative rim charges. This forward rotation can increase a water velocity when the charge is small. Moreover, more water molecules can enter into the channel per unit time. Waters gaining enough kinetic energy (Figure 3c) have higher passage rates (Figure 7a). If the charge is too large, stronger Coulomb forces will hold water around the pore edge and hinder them from passing through the membrane.

On the contrary, positive charges change the dipole orientation from +dipole states to −dipole states. This reversed water orientation to the $-z$-direction can slow down the passage of water molecules for a weak rim charging (Figure 3d). A small kinetic energy of water makes it more difficult to overcome the energy barrier (Figure 7b), which is causing the water flux to decline. For rims with a larger positive charging, the strong Coulomb coupling between water molecules and the rim atoms largely prevents water from permeating through the pore, but it does not entirely block the pore. Since more water molecules are at the same time attracted by the strong interaction, most

DOI: 10.1021/acs.jpcc.9b09238
J. Phys. Chem. C 2019, 123, 27690−27696

water come back to the feed side (Figure 7b). Thus, the water flux almost stays constant for high charging of the rim.

In Figures 2 and S4, a larger water flux is found across flexible pores, which can catch more waters (Table 1). Although most of the waters are released back to the feed reservoir, resulting in a low water transmembrane probability, more water molecules permeate through the membrane than through the fixed pores (Table 1). Moreover, the membrane fluctuations result in effective increasing of the pore size, since the pore edge atoms are not in the same plane (Figure S9 and Table S2). The pore sizes were evaluated by using the Multiwfn software.[52] With increasing partial atomic charges, the conformational change of the membrane structure in the solution becomes more and more obvious (Figure S9), changing the ultrathin pore from a plane to a three-dimensional irregular conical cavity (Figure S10). This structural change is beneficial for more water molecules passing through the flexible pore. Figure S11 shows that water density within the flexible B5 and N5 pores is higher than within the same fixed pores. Moreover, the stability of hydrogen bonds around water molecules in tubular channels is better than within single-layer nanoporous membranes.[5] In-Interstingly, in more polar flexible pores, no significant breaking of hydrogen bonds occurs when water molecules pass across the irregular conical cavity (Figure S12). Thus, water molecules can relatively smoothly pass through the flexible pore.

Table 1. Number of Water Molecules and Passage Probability for Flexible and Fixed Membranes in the initial 10 ns (Steady-State Flow)

	N_{wp}	N_{wr}	N_{wt}	P_T (%)
N5-fixed (q = 0)	504	707	1211	41.61
N5-flexible (q = 0)	688	1962	2630	25.39
B5 fixed ($\|q\|$ = 0.1)	473	679	1152	41.05
B-flexible ($\|q\|$ = 0.1)	522	1939	2461	21.21

IV. CONCLUSIONS

In summary, using MD simulations, we have studied water transport through nanopores with highly polar rims. We found that the rim charges can significantly modify the effective pore cross-sections and water fluxes, so that the behavior of water can be very sensitive to Coulomb forces acting in such a short channel. The simulations also demonstrated that when it comes to interactions with water, negatively charged rims have effectively a longer interaction radius to catch water hydrogens than positively charged rims in catching water oxygens. Therefore, the negatively charged pore rims can significantly increase the pore cross-sections. The observed phenomena can have numerous applications in water transport, desalination, and molecular separation.

■ ASSOCIATED CONTENT

Supporting Information

The Supporting Information is available free of charge on the ACS Publications website at DOI: 10.1021/acs.jpcc.9b09238.

Charges and Lennard-Jones parameters; water density along the z-direction of F-pore and H-pore; number of net permeated water molecules across fixed B5 and N5 membrane; water flux passing through fixed and flexible nanopores at different pressures; Coulomb interaction energy between water molecules and membrane atoms (PDF)

■ AUTHOR INFORMATION

Corresponding Authors

*E-mail: pkral@uic.edu (P.K.).
*E-mail: rflu@njust.edu.cn (R.L.).

ORCID

Petr Král: 0000-0003-2992-9027
Ruifeng Lu: 0000-0002-1752-2070

Notes

The authors declare no competing financial interest.

■ ACKNOWLEDGMENTS

The research was financially supported by NSF of China Grant No. 11747029, Fundamental Research Funds for the Central Universities (No. 30916011105), Natural Science Foundation of Jiangsu Province (No. BK20170032). P.K. was supported by the NSF DMR-1506886 grant. H.G. also acknowledges the support from the program of China Scholarship Council (CSC).

■ REFERENCES

(1) Hillie, T.; Hlophe, M. Nanotechnology and the Challenge of Clean Water. *Nat. Nanotechnol.* **2007**, *2*, 663−664.
(2) Xu, G.-R.; Xu, J. M.; Su, H. C.; Liu, X. Y.; Lu, L.; Zhao, H. L.; Feng, H. J.; Das, R. Two-Dimensional (2d) Nanoporous Membranes with Sub-Nanopores in Reverse Osmosis Desalination: Latest Developments and Future Directions. *Desalination* **2019**, *451*, 18−34.
(3) Wang, L.; Boutilier, M. S. H.; Kidambi, P. R.; Jang, D.; Hadjiconstantinou, N. G.; Karnik, R. Fundamental Transport Mechanisms, Fabrication and Potential Applications of Nanoporous Atomically Thin Membranes. *Nat. Nanotechnol.* **2017**, *12*, 509−522.
(4) Sint, K.; Wang, B.; Král, P. Selective Ion Passage through Functionalized Graphene Nanopores. *J. Am. Chem. Soc.* **2008**, *130*, 16448−16449.
(5) Suk, M. E.; Aluru, N. R. Water Transport through Ultrathin Graphene. *J. Phys. Chem. Lett.* **2010**, *1*, 1590−1594.
(6) Cohen-Tanugi, D.; Grossman, J. C. Water Desalination across Nanoporous Graphene. *Nano Lett.* **2012**, *12*, 3602−3608.
(7) Wang, Y.; He, Z.; Gupta, K. M.; Shi, Q.; Lu, R. Molecular Dynamics Study on Water Desalination through Functionalized Nanoporous Graphene. *Carbon* **2017**, *116*, 120−127.
(8) Heiranian, M.; Farimani, A. B.; Aluru, N. R. Water Desalination with a Single-Layer Mos2 Nanopore. *Nat. Commun.* **2015**, *6*, No. 8616.
(9) Ang, E. Y. M.; Ng, T. Y.; Yeo, J.; Liu, Z.; Geethalakshmi, K. R. Free-Standing Graphene Slit Membrane for Enhanced Desalination. *Carbon* **2016**, *110*, 350−355.
(10) Gao, H.; Shi, Q.; Rao, D.; Zhang, Y.; Su, J.; Liu, Y.; Wang, Y.; Deng, K.; Lu, R. Rational Design and Strain Engineering of Nanoporous Boron Nitride Nanosheet Membranes for Water Desalination. *J. Phys. Chem. C* **2017**, *121*, 22105−22113.
(11) Corry, B. Water and Ion Transport through Functionalised Carbon Nanotubes: Implications for Desalination Technology. *Energy Environ. Sci.* **2011**, *4*, 751.
(12) Shi, Q.; Gao, H.; Zhang, Y.; Meng, Z.; Rao, D.; Su, J.; Liu, Y.; Wang, Y.; Lu, R. Bilayer Graphene with Ripples for Reverse Osmosis Desalination. *Carbon* **2018**, *136*, 21−27.
(13) Li, W.; Wang, W.; Zhang, Y.; Yan, Y.; Král, P.; Zhang, J. Highly Efficient Water Desalination in Carbon Nanocones. *Carbon* **2018**, *129*, 374−379.
(14) Shi, Q.; Zhang, K.; Lu, R.; Jiang, J. Water Desalination and Biofuel Dehydration through a Thin Membrane of Polymer of

DOI: 10.1021/acs.jpcc.9b09238
J. Phys. Chem. C 2019, 123, 27690−27696

Intrinsic Microporosity: Atomistic Simulation Study. *J. Membr. Sci.* **2018**, *545*, 49−56.
(15) Xu, W. L.; Fang, C.; Zhou, F.; Song, Z.; Liu, Q.; Qiao, R.; Yu, M. Self-Assembly: A Facile Way of Forming Ultrathin, High-Performance Graphene Oxide Membranes for Water Purification. *Nano Lett.* **2017**, *17*, 2928−2933.
(16) Yan, Y.; Li, W.; Král, P. Enantioselective Molecular Transport in Multilayer Graphene Nanopores. *Nano Lett.* **2017**, *17*, 6742−6746.
(17) Chen, L.; Shi, G.; Shen, J.; Peng, B.; Zhang, B.; Wang, Y.; Bian, F.; Wang, J.; Li, D.; Qian, Z.; et al. Ion Sieving in Graphene Oxide Membranes Via Cationic Control of Interlayer Spacing. *Nature* **2017**, *550*, 380−383.
(18) Hong, S.; Constans, C.; Surmani Martins, M. V.; Seow, Y. C.; Guevara Carrio, J. A.; Garaj, S. Scalable Graphene-Based Membranes for Ionic Sieving with Ultrahigh Charge Selectivity. *Nano Lett.* **2017**, *17*, 728−732.
(19) He, Z. J.; Zhou, J.; Lu, X. H.; Corry, B. Bioinspired Graphene Nanopores with Voltage-Tunable Ion Selectivity for Na+ and K+. *ACS Nano* **2013**, *7*, 10148−10157.
(20) Esfandiar, A.; Radha, B.; Wang, F.; Yang, Q.; Hu, S.; Garaj, S.; Nair, R.; Geim, A.; Gopinadhan, K. Size Effect in Ion Transport through Angstrom-Scale Slits. *Science* **2017**, *358*, 511−513.
(21) Hao, L.; Su, J.; Guo, H. Water Permeation through a Charged Channel. *J. Phys. Chem. B* **2013**, *117*, 7685−7694.
(22) Hilder, T. A.; Gordon, D.; Chung, S. H. Salt Rejection and Water Transport through Boron Nitride Nanotubes. *Small* **2009**, *5*, 2183−2190.
(23) Rikhtehgaran, S.; Lohrasebi, A. Water Desalination by a Designed Nanofilter of Graphene-Charged Carbon Nanotube: A Molecular Dynamics Study. *Desalination* **2015**, *365*, 176−181.
(24) Secchi, E.; Marbach, S.; Nigues, A.; Stein, D.; Siria, A.; Bocquet, L. Massive Radius-Dependent Flow Slippage in Carbon Nanotubes. *Nature* **2016**, *537*, 210−213.
(25) Wang, B.; Kŕal, P. Coulombic Dragging of Molecules on Surfaces Induced by Separately Flowing Liquids. *J. Am. Chem. Soc.* **2006**, *128*, 15984−15985.
(26) Tocci, G.; Joly, L.; Michaelides, A. Friction of Water on Graphene and Hexagonal Boron Nitride from Ab Initio Methods: Very Different Slippage Despite Very Similar Interface Structures. *Nano Lett.* **2014**, *14*, 6872−6877.
(27) Won, C. Y.; Aluru, N. R. Structure and Dynamics of Water Confined in a Boron Nitride Nanotube. *J. Phys. Chem. C* **2008**, *112*, 1812−1818.
(28) Garnier, L.; Szymczyk, A.; Malfreyt, P.; Ghoufi, A. Physics Behind Water Transport through Nanoporous Boron Nitride and Graphene. *J. Phys. Chem. Lett.* **2016**, *7*, 3371−3376.
(29) Zhu, F.; Tajkhorshid, E.; Schulten, K. Pressure-Induced Water Transport in Membrane Channels Studied by Molecular Dynamics. *Biophys. J.* **2002**, *83*, 154−160.
(30) Huang, C.; Nandakumar, K.; Choi, P. Y.; Kostiuk, L. W. Molecular Dynamics Simulation of a Pressure-Driven Liquid Transport Process in a Cylindrical Nanopore Using Two Self-Adjusting Plates. *J. Chem. Phys.* **2006**, *124*, No. 234701.
(31) Takaba, H.; Onumata, Y.; Nakao, S. Molecular Simulation of Pressure-Driven Fluid Flow in Nanoporous Membranes. *J. Chem. Phys.* **2007**, *127*, No. 054703.
(32) Wang, L.; Dumont, R. S.; Dickson, J. M. Nonequilibrium Molecular Dynamics Simulation of Water Transport through Carbon Nanotube Membranes at Low Pressure. *J. Chem. Phys.* **2012**, *137*, No. 044102.
(33) Li, W.; Yang, Y.; Weber, J. K.; Zhang, G.; Zhou, R. Tunable, Strain-Controlled Nanoporous Mos(2) Filter for Water Desalination. *ACS Nano* **2016**, *10*, 1829−1835.
(34) Strong, S. E.; Eaves, J. D. The Dynamics of Water in Porous Two-Dimensional Crystals. *J. Phys. Chem. B* **2017**, *121*, 189−207.
(35) Strong, S. E.; Eaves, J. D. Atomistic Hydrodynamics and the Dynamical Hydrophobic Effect in Porous Graphene. *J. Phys. Chem. Lett.* **2016**, *7*, 1907−1912.
(36) Abraham, M. J.; Murtola, T.; Schulz, R.; Páll, S.; Smith, J. C.; Hess, B.; Lindahl, E. Gromacs: High Performance Molecular Simulations through Multi-Level Parallelism from Laptops to Supercomputers. *SoftwareX* **2015**, *1−2*, 19−25.
(37) Jorgensen, W. L.; Chandrasekhar, J.; Madura, J. D.; Impey, R. W.; Klein, M. L. Comparison of Simple Potential Functions for Simulating Liquid Water. *J. Chem. Phys.* **1983**, *79*, 926−935.
(38) Essmann, U.; Perera, L.; Berkowitz, M. L.; Darden, T.; Lee, H.; Pedersen, L. G. A Smooth Particle Mesh Ewald Method. *J. Chem. Phys.* **1995**, *103*, 8577−8593.
(39) Bussi, G.; Donadio, D.; Parrinello, M. Canonical Sampling through Velocity Rescaling. *J. Chem. Phys.* **2007**, *126*, No. 014101.
(40) Lee, C. S.; Choi, M. K.; Hwang, Y. Y.; Kim, H.; Kim, M. K.; Lee, Y. J. Facilitated Water Transport through Graphene Oxide Membranes Functionalized with Aquaporin-Mimicking Peptides. *Adv. Mater.* **2018**, *30*, No. e1705944.
(41) Humphrey, W.; Dalke, A.; Schulten, K. Vmd: Visual Molecular Dynamics. *J. Mol. Graphics* **1996**, *14*, 33−38.
(42) Melillo, M.; Zhu, F.; Snyder, M. A.; Mittal, J. Water Transport through Nanotubes with Varying Interaction Strength between Tube Wall and Water. *J. Phys. Chem. Lett.* **2011**, *2*, 2978−2983.
(43) Lei, W.; Portehault, D.; Liu, D.; Qin, S.; Chen, Y. Porous Boron Nitride Nanosheets for Effective Water Cleaning. *Nat. Commun.* **2013**, *4*, No. 1777.
(44) Liu, H.; Wang, H.; Zhang, X. Facile Fabrication of Freestanding Ultrathin Reduced Graphene Oxide Membranes for Water Purification. *Adv. Mater.* **2015**, *27*, 249−254.
(45) Kang, J. W.; Hwang, H. J. Comparison of C60encapsulations into Carbon and Boron Nitride Nanotubes. *J. Phys.: Condens. Matter* **2004**, *16*, 3901−3908.
(46) Jin, C.; Lin, F.; Suenaga, K.; Iijima, S. Fabrication of a Freestanding Boron Nitride Single Layer and Its Defect Assignments. *Phys. Rev. Lett.* **2009**, *102*, No. 195505.
(47) Wang, C.; Wen, B.; Tu, Y.; Wan, R.; Fang, H. Friction Reduction at a Superhydrophilic Surface: Role of Ordered Water. *J. Phys. Chem. C* **2015**, *119*, 11679−11684.
(48) Ostrowski, J. H.; Eaves, J. D. The Tunable Hydrophobic Effect on Electrically Doped Graphene. *J. Phys. Chem. B* **2014**, *118*, 530−536.
(49) Tan, S. F.; Raj, S.; Bisht, G.; Annadata, H. V.; Nijhuis, C. A.; Král, P.; Mirsaidov, U. Nanoparticle Interactions Guided by Shape-Dependent Hydrophobic Forces. *Adv. Mater.* **2018**, *30*, No. 1707077.
(50) Gupta, K. M.; Qiao, Z.; Zhang, K.; Jiang, J. Seawater Pervaporation through Zeolitic Imidazolate Framework Membranes: Atomistic Simulation Study. *ACS Appl. Mater. Interfaces* **2016**, *8*, 13392−13399.
(51) Su, J.; Guo, H. Control of Unidirectional Transport of Single-File Water Molecules through Carbon Nanotubes in an Electric Field. *ACS Nano* **2011**, *5*, 351−359.
(52) Lu, T.; Chen, F. Multiwfn: A Multifunctional Wavefunction Analyzer. *J. Comput. Chem.* **2012**, *33*, 580−592.

DOI: 10.1021/acs.jpcc.9b09238
J. Phys. Chem. C 2019, 123, 27690−27696